Preprint Cambridge Centre for Computational Chemical Engineering ISSN 1473 – 4273

Investigation of the impact of the configuration of exhaust after-treatment system for diesel engines

Chung Ting Lao[1], Jethro Akroyd[1,5], Nickolas Eaves[1,2], Alastair Smith[3], Neal Morgan[3], Daniel Nurkowski[4], Amit Bhave[4], Markus Kraft[1,5,6]

released: May 21, 2019

[1] Department of Chemical Engineering and Biotechnology
University of Cambridge
Philippa Fawcett Drive
Cambridge, CB3 0AS
United Kingdom

E-mail: mk306@cam.ac.uk

[2] Mechanical, Automotive and Materials Engineering
University of Windsor
401 Sunset Avenue
Windsor, ON, N9B 3P4
Canada

[3] Shell Centre
York Road
London, SE1 7NA
United Kingdom

[4] CMCL Innovations
Sheraton House
Cambridge, CB3 0AX
United Kingdom

[5] CARES
Cambridge Centre for Advanced Research and Education in Singapore
1 Create Way
CREATE Tower, #05-05
Singapore, 138602

[6] School of Chemical and Biomedical Engineering
Nanyang Technological University
62 Nanyang Drive
Singapore, 637459

Preprint No. 228

UNIVERSITY OF CAMBRIDGE

Keywords: Exhaust After-Treatment (EAT), Diesel oxidation catalyst (DOC), Ammonia-based Selective Catalytic Reduction (NH_3-SCR), Diesel Particulate Filter (DPF), Numerical model

Edited by
Computational Modelling Group
Department of Chemical Engineering and Biotechnology
University of Cambridge
Philippa Fawcett Drive
Cambridge CB3 0AS
United Kingdom

E-Mail: c4e@cam.ac.uk
World Wide Web: http://como.ceb.cam.ac.uk/

Abstract

Exhaust After-Treatment (EAT) systems are necessary for automotive powertrains to meet stringent emission standards. Computational modelling has been applied to aid designing EAT systems. Models with global kinetic mechanisms are often used in practice, but they cannot accurately predict the behaviour of after-treatment devices under a wide range of conditions. In this study, a numerical EAT model with rigorous treatment of the catalytic chemistry is proposed to investigate the impact of the configuration of individual devices in the EAT system; one of the key design decisions. The performance of the proposed model is first critically assessed against experimental and simulation data from the literature before being applied to design a multi-device EAT system for a diesel engine. The target EAT system is composed of a diesel oxidation catalyst (DOC), an ammonia-based selective catalytic reduction (NH_3-SCR) device and a diesel particulate filter (DPF). The steady state behaviour of various EAT designs under operating conditions across the engine map are examined. The DOC-DPF-SCR layout is found to be more beneficial than the alternative DOC-SCR-DPF for the specific engine studied. Furthermore, the DPF-front system is more robust with respect to changes in emission regulations. Flux analysis is applied to study the chemical interaction in the SCR and explain the disadvantage of the SCR-front system. In addition, it is demonstrated in the study that future catalyst investigations should consider more realistic feed compositions.

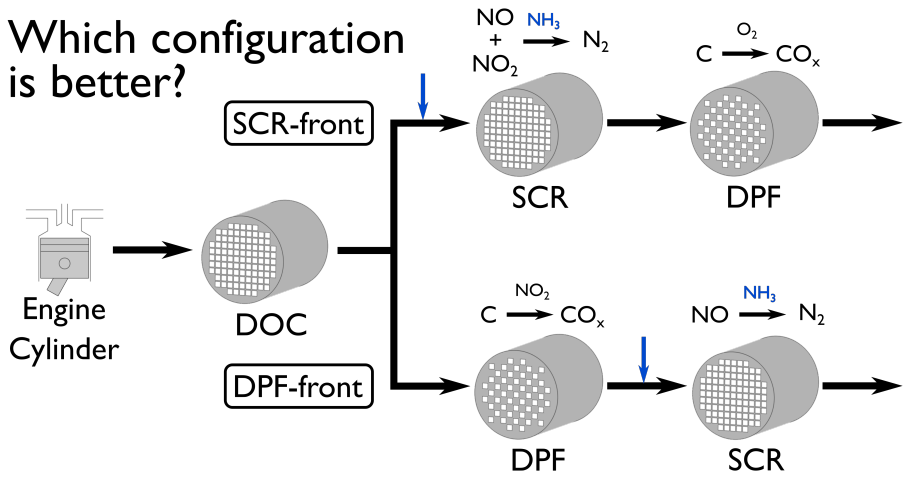

Highlights

- Development of after-treatment model with rigorous treatment of catalytic chemistry
- Investigation of the chemical interactions between after-treatment devices
- The "DPF-front" configuration is found to perform better under steady state operation

Contents

1 Introduction

Internal Combustion Engines (ICEs) are widely used to provide power for vehicles [26]. In 2018, vehicles with ICEs powered by petrol and diesel made up over 90% of the new passenger car registrations in the European Union (EU) [2], and in particular, 96% of heavy-duty engines in EU are powered by diesel [3]. However, emissions from ICE containing carbon monoxide (CO), unburnt hydrocarbon (uHC), nitrogen oxides (NOx) and particulate matter (PM) can cause adverse impacts on human health and the environment [30, 41, 52, 60]. Correspondingly, governing bodies have set legal limits on ICE emissions that manufacturers must meet.

Since tailpipe emissions depend on the operating conditions of the ICE, the engine "test cycle" must be clearly defined such that the emission measurements are repeatable [27]. However, it has been found that emission measurements using simple test cycles such the New European Driving Cycle (NEDC) are not representative of the actual on-road emissions [61]. And as a result, more realistic test cycles such as the Worldwide Harmonized Light Vehicles Test Cycle (WLTC) have been introduced [61]. In addition, Real Driving Emission (RDE) testing will be implemented, in which tailpipe emissions are measured when the vehicle is operating on-road [60].

Exhaust After-Treatment (EAT) is an important part of emission control of ICEs. Other emission control technologies, such as exhaust gas recirculation (EGR) and alternative fuel formulations, have also been applied by manufacturers to meet the increasingly stringent emission standards [25]. In contrast to other emission control technologies, the EAT system has a smaller impact on the in-cylinder combustion. It is placed between the engine cylinders and the tailpipe in a vehicle where it reduces the regulated substances in the engine-out exhaust.

Typical EAT systems for diesel engines are composed of three individual devices [22]. Diesel EAT systems usually contain two Flow-Through Monoliths (FTMs) with a catalytic coating on the channel walls for the mitigation of gaseous pollutants. The structure of a typical FTM is shown in Fig. 1(a). The purpose of the Diesel Oxidation Catalyst (DOC) is to oxidise CO and uHC to form CO_2 and H_2O [4]. In addition to the DOC, a separate FTM is required for NOx control. The reduction of NOx to nitrogen (N_2) is difficult due to the high level of oxygen (O_2) in diesel exhaust [18]. Two technologies are commonly applied to reduce NOx emission, namely the Lean NOx Trap (LNT) and the Selective Catalytic Reduction (SCR) device. In this work, we focus on the SCR technology since it is the preferred deNOx technology for heavy-duty applications [21, 56]. The SCR is able to reduce NOx to N_2 at high oxygen levels with the aid of an additional reductant. The most popular of which is ammonia (NH_3) [54], stored in the form of urea solution. During operation, urea is injected into the exhaust flow and NH_3 is formed from the decomposition of urea [4]. SCR with alternative reductants, for example hydrocarbon [31] and CO [16], are also possible.

Whilst catalytic FTMs are effective for controlling toxic gaseous emissions, Diesel Particulate Filters (DPFs) are required to control particulate emissions. DPFs have a Wall-Flow Monolith (WFM) structure as shown in Fig. 1(b). As opposed to having open channels like the FTM, the ends of channels in a WFM are alternately plugged. Particulates in the

exhaust accumulate in the porous wall between channels when exhaust flows through the device. The backpressure in the DPF will increase during operation due to accumulation of particles in the device. This leads to worse in-cylinder combustion performance, and hence trapped particles are removed by "regeneration", which is the combustion of the carbonaceous part of trapped particles.

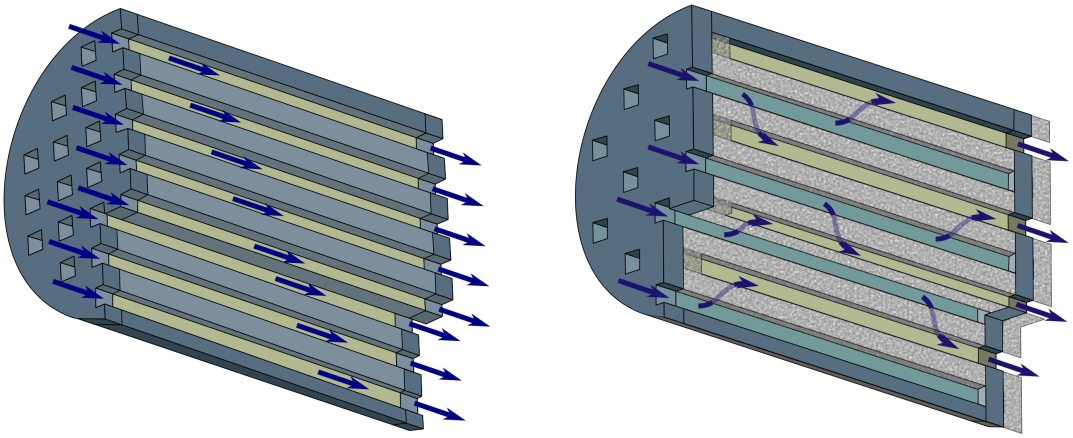

(a) Flow Through Monolith (FTM). (b) Wall Flow Monolith (WFM).

Figure 1: *The structures of a Flow Through Monolith (FTM) and a Wall Flow Monolith (WFM) are shown.*

Regeneration strategies can be categorised as either "active" or "passive". During active regeneration, the temperature of the DPF is increased temporarily by the means of altering engine operation or external fuel injection [34]. Trapped particles are then be burnt by O_2 at above 500°C [6]. For passive regeneration, trapped particles are oxidised by NO_2, a much more powerful oxidant than O_2. The reaction is spontaneous at typical diesel exhaust temperatures (300°C [64]). A balance between filtration and passive regeneration may be reached without an additional heat source and hence passive regeneration is more favourable than active regeneration strategies since it has a lower associated fuel penalty [53].

Since more than one EAT device is required, there are several possible combinations of individual devices in the EAT system. It is important to understand the synergistic and competitive interactions between EAT devices in order to choose the optimal configuration for a certain engine. The DOC is usually the first device in the system due to its beneficial impact on downstream devices. First of all, the thermal energy released from exothermic reactions occurring inside the DOC can warm up downstream devices. This can help reduce tailpipe emission during cold-start of engines due to catalyst inactivity at low temperature [32]. Furthermore, the DOC is able to convert NO to NO_2 as well as oxidising CO and uHC [28]. NO_2 generated from the DOC can assist passive regeneration in the DPF. The deNOx performance in the SCR can be improved if the NO_2/NOx ratio is increased [14]. The DOC is also used to initiate active regeneration in the DPF, for example raising the temperature of exhaust by oxidising injected fuel [55].

On the other hand, the interactions between the DPF and the SCR are mainly competitive.

If the DPF is placed in front of the SCR ("DPF-front"), the SCR will warm up more slowly during cold-start period as the DPF acts as a heat sink [24]. Passive regeneration in the DPF would consume NO_2 in the exhaust, preventing maximum deNOx performance in the downstream SCR. Furthermore, the downstream SCR is vulnerable to the heat generated from active regeneration in the DPF. In spite of these negative influences on SCR performance, the upstream DPF can reduce particle fouling on the wall of the downstream SCR [23]. Depending on the economic analysis, it may be preferable to have a "SCR-front" system, where the performance of the SCR is better, at the expense of suppressing passive regeneration in the downstream DPF, resulting in increased fuel consumption [22].

Given the complexity of the processes and interactions within EAT system, computational models are widely used to study and optimise the designs [4]. The performance of the EAT system is affected by numerous phenomena, including gas flow, heat and mass transfer, chemical reaction as well as particle filtration. Furthermore, each channel in a EAT device may behave differently depending on the inlet conditions and the relative positions of the channels inside the monolith. Depending on the purpose of the model, various simplifications of the model may be made to lower the computing cost while maintaining sufficient accuracy [12]. For example, the overall behaviour of a EAT device may be described by simulating a single representative channel with reasonable accuracy instead of simulating every channel in the monolith [17].

One of the difficulties in EAT modelling arises from the complex reaction mechanisms of the catalyst. Simple "global kinetic" mechanisms with semi-empirical reaction rate expressions (based on work of Voltz et al. [62] for example) are often used. However they are rarely able to describe transient behaviour e.g. when the inlet composition changes [37]. The global kinetic approach is also unable to describe the composition profile of species adsorbed on the catalyst which can have significant impact [46]. The capability of handling detailed microkinetic mechanisms based on elementary reactions is desirable for after-treatment models because of increasingly stringent emission testing procedures and emission standards. Furthermore, such models can allows better understanding of the intrinsic kinetics of the catalyst, which is especially useful for investigation of new catalyst formulations for the next-generation after-treatment technology.

This paper aims to propose a computational EAT model that allows a rigorous treatment for the catalytic chemistry unlike black-box models provided by most manufacturers [4]. Such a model can offer more insight into the chemical phenomena in the EAT system, and shed light on the interaction between individual devices. This work focuses on the steady state of the after-treatment system for two main reasons. First, steady state operation is a good indication of sufficient passive regeneration, an important phenomena for multi-device EAT system for diesel engines. Second, transient behaviour of an EAT system can be influenced by thermal effects and past operations, which would make it more difficult to evaluate the impact of chemical interactions.

The rest of this paper is structured as follows: The governing equations of the proposed model and the numerical methods used are described in Section 2. The proposed model is then applied to simulate individual EAT devices. The results are compared with experimental and simulation data from the literature in Section 3. After that, the proposed model is integrated with a virtual engine cylinder simulation software in Section 4 to investigate the advantages and disadvantages of DPF-front and SCR-front systems via a case study

of a heavy-duty diesel engine. Finally, element flux analysis is applied in Section 4.2.3 to study the chemical phenomena in the EAT system.

2 Model description

This section is split into two parts. The first part describes the governing equations of the after-treatment model. The second part describes the coupling between the engine in-cylinder combustion model and the after-treatment model.

2.1 Governing equations

The model used in this work is a modified version of the WFM model described in detail by Lao et al. [40]. The key equations used in this work is summarised below.

The single channel approach is applied in this study to simulate EAT devices. It assumes that all channels in the monolith have the same behaviour. A single FTM channel is described by a one-dimensional model, where variations in radial direction are neglected. The spatial representation of a FTM in the model is shown in Fig. 2(a). For WFM, a pair of inlet and outlet channels, as well as the porous wall in between, are modelled [40]. The channels are discretised in the axial direction. The porous wall is discretised in the through-wall direction in addition to the axial direction. The spatial representation of a WFM in the model is shown in Fig. 2(b). Ideal gas behaviour has been assumed for the gas phase mixture.

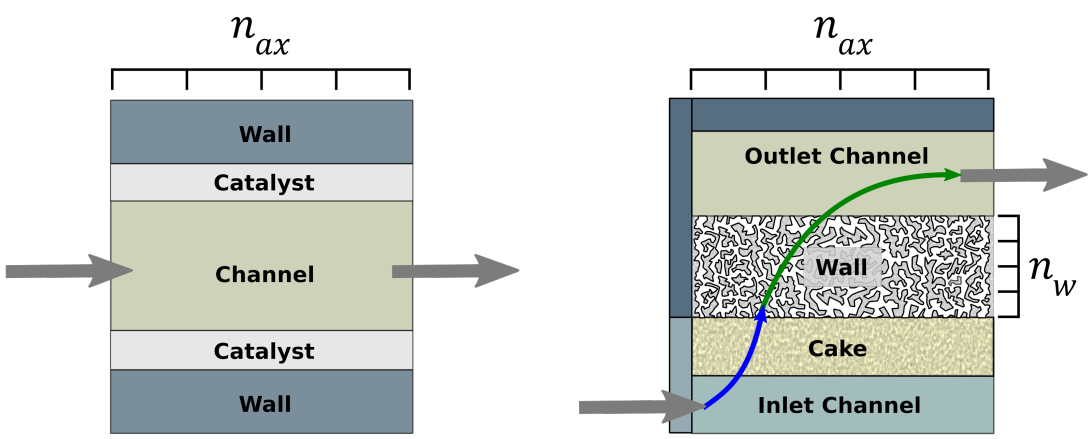

(a) Flow Through Monolith (FTM). (b) Wall Flow Monolith (WFM).

Figure 2: *The spatial representations of a FTM and a WFM in the model.*

The gas flows along the channels of FTMs and WFMs are governed by the Bernoulli's equation, whereas the gas flows in the through-wall direction across the particle cake layer and the porous wall in WFMs are governed by Darcy's Law. The variation of gas pressure

along channels and across porous medium are described by eq. (1) and (2) respectively [40]:

$$P_{\text{in}} + \frac{1}{2}\rho_{\text{in}} u_{\text{in}}^2 = P_{\text{out}} + \frac{1}{2}\rho_{\text{out}} u_{\text{out}}^2 + \frac{F \mu L_{\text{channel}}}{D^2} u_{\text{out}}, \tag{1}$$

$$P_{\text{in}} - P_{\text{out}} = \frac{\mu v L_{\text{porous medium}}}{\kappa}, \tag{2}$$

where P is pressure, ρ is gas mass density, u is gas flow velocity in a channel, F is a friction factor ($= 28.454$ for square channel [57]), μ is dynamic viscosity, L is the distance between volume elements, D is the side length of the cross-section of a square channel, v is the gas flow velocity across porous media and κ is the permeability of the porous medium. The subscripts "in" and "out" denote adjacent upstream and downstream volume elements respectively.

The model proposed by this work can describe the composition of the gas phase and the "surface" phase i.e. adsorbed species on the reactive surface of the catalyst. The composition of the gas phase is affected by the gas flow and chemical reactions. The governing equation of the gas phase species is shown below [40]:

$$\frac{\mathrm{d}n_{\gamma,i}}{\mathrm{d}t} = \sum_{j \in S_{\text{in},i}} \frac{\dot{m}_j Y_{\gamma,\text{in},j}}{M_\gamma} - \sum_{j \in S_{\text{out},i}} \frac{\dot{m}_j Y_{\gamma,i}}{M_\gamma} + V_i \sum_{w=1}^{W} \nu_{\gamma,w} r_{w,i}, \tag{3}$$

where n is the number of mole of a gas species, $\dot{m}$ is the gas mass flow rate, Y is the mass fraction, M is the molar mass of a gas species, V is the volume of a volume element, ν is the stoichiometric coefficient of a species in a reaction and r is the rate of reaction, γ is the index of gas phase species, i is the index of volume elements, j is the index of connection between two volume elements which allows gas flow, w is the index of reactions, $S_{\text{in},i}$ is the set of all inflow connections to volume element i, $S_{\text{out},i}$ is the set of all outflow connections to volume element i and W is the total number of reactions. Convective mass transfer phenomena are not included in the proposed model because they are greatly dependent on operating conditions. Inclusion of these phenomena in the model would lead to additional calibrations and uncertainties with limited benefit on the investigation of chemical interaction between after-treatment devices. The impact of this modelling decision is discussed in Section 3.

The composition of surface species is described by eq. (4) below:

$$\frac{\mathrm{d}n_{\beta,i}}{\mathrm{d}t} = V_i \sum_{w=1}^{W} \nu_{\beta,w} r_{w,i}, \tag{4}$$

where β is the index of surface phase species. Adsorption and desorption of species are described as chemical reactions which is a common practice for EAT modelling [for example 36, 49]. A micro-kinetic approach is used for the treatment of the chemistry to allow the application of a detailed kinetic mechanism. The rate of a reaction is based on an Arrhenius-type equation, with capability of considering user-specified reaction order

and coverage dependency of activation energy [50]. The rate of a reaction r is calculated as follows:

$$r_{w,i} = \eta k_{w,i} \prod_{\gamma=1}^{\Gamma} c_{\gamma,i}^{X_{\gamma,w}} \prod_{\beta=1}^{\Psi} \left(\frac{S_i}{V_i} \zeta_{\beta,i} \right)^{X_{\beta,w}}, \tag{5}$$

$$k_{w,i} = A_w T_i^{B_w} \exp\left(-\frac{E_w}{RT_i} \right) \prod_{\beta=1}^{\Psi} \exp\left(\frac{-\sigma_{\beta,w}\theta_{\beta,i}}{RT_i} \right), \tag{6}$$

where $c_{\gamma,i}$ is the molar concentration of gas species, Γ is the total number of gas phase species, X is the reaction order of a gas species, S is the reactive surface area in a volume element, ζ is the surface concentration of a surface species, Ψ is the total number of surface phase species, A is the pre-exponential constant, B is the temperature exponent and E is the activation energy of a reaction. A global effectiveness factor η is applied as a tunable constant to describe the effect of internal diffusion in the catalytic washcoat. The coverage dependency is represented by the product of exponentials on the right hand side of eq. (6) where σ and θ are a coverage dependent parameter and site fraction of a surface species respectively.

A sectional method is applied to numerically solve the particle size distribution in after-treatment devices [40]. The number density of trapped particles $N_{z,i}$ of size class z in the porous wall volume element i is governed by the following equation:

$$\frac{\mathrm{d}N_{z,i}}{\mathrm{d}t} = Q_{z,i}\dot{N}_{z,\mathrm{in}} + \left(k_{\mathrm{AR}}\left[\mathrm{O_2}\right] + k_{\mathrm{PR}}\left[\mathrm{NO_2}\right]\right)\left(\pi d_{\mathrm{p},z}^2 N_{z,i}\right), \tag{7}$$

where $Q_{z,i}$ is the filtration efficiency of particles of size class z, $\dot{N}_{z,\mathrm{in}}$ is the inlet flow rate of particle number density and $d_{\mathrm{p},z}$ is the diameter of particle in size class z. $Q_{z,i}$ is calculated using the classic unit collector model [33]. It is described in detail elsewhere [40, Section 2.2]. The extended features developed by Lao et al. [40] are not included in this work since those features are applied to describe the transient behaviour of active regenerating DPFs, which is beyond the scope of this work.

The model used in this work considers passive regeneration by NO_2 in addition to active regeneration by O_2. k_{AR} and k_{PR} are the rate constants for active and passive regeneration reactions with Arrhenius form as shown in eq. 6. The following regeneration reactions are considered in the model:

$$\mathrm{C} + \alpha_1 \mathrm{O_2} \rightarrow (2\alpha_1 - 1)\,\mathrm{CO_2} + (2 - 2\alpha_1)\,\mathrm{CO}, \tag{8}$$

$$\mathrm{C} + \alpha_2 \mathrm{NO_2} \rightarrow \alpha_2 \mathrm{NO} + (\alpha_2 - 1)\,\mathrm{CO_2} + (2 - \alpha_2)\,\mathrm{CO}, \tag{9}$$

where α_1 and α_2 are stoichiometric coefficients of the regeneration reactions. Different literatures [33, 35, 47, 57] suggest different values of αs and their temperature dependences. In this study, α_1 and α_2 take constant values of 0.8 and 1.8 respectively ,within the possible range suggested in literature [28].

The thermal behaviour of the EAT system is neglected in the model used in this work. This is justified for three reasons: First, the thermal behaviour has more prominence on the transient behaviour such as cold-start and active regeneration, whereas this study focuses on steady state investigation as stated in Section 1. Second, the heat of reaction in SCR is usually negligible [49]. It is found by Schejbal et al. [58] that the same applies to the DOC and passively regenerating DPF. Third, heat loss to the environment can be limited by having insulation packing around EAT devices. Whilst such heat loss can be modelled [for example eq. (53) of 33], it leads to additional design parameters without bringing additional benefits for the investigation. Therefore the heat balance equation is omitted in this model assuming insulations are appropriately designed to minimise heat loss of the EAT system. As a result, the temperature of the EAT system is that of the inlet flow.

2.2 Coupling with engine model

The Stochastic Reactor Model (SRM) Engine Suite [15] is used to specify the inlet boundary conditions to the EAT system. The SRM Engine Suite can predict the cylinder-out mass flow rate, gas composition and temperature of the exhaust using a Probability Density Function (PDF) based model [8]. It has been shown to be a computationally efficient tool for internal combustion engine simulations [5, 7–9, 19, 38, 39, 42–45, 63].

Whilst the mass flow rate and gas composition should remain unchanged from the cylinder to the inlet of the EAT system, there is significant heat loss when the exhaust passes from engine cylinders to the EAT system through the turbocharger and pipings. It is possible to apply a detailed model such as the one described by Payri et al. [51] to estimate the heat loss process. However it would require additional information such as the geometry of the turbocharger. The application of such a model and design of pipings of the engine system is out of the scope of this work. Here we seek a simple equation that gives realistic estimation of the inlet temperature of the EAT system (between 200°C and 500°C [20]) based on the cylinder temperature. By treating the pipings between engine cylinders and after-treatment system as a cylinder, we have the following energy balance equation:

$$\dot{m}C_{\mathrm{p,cyn}}T_{\mathrm{cyn}} = \dot{m}C_{\mathrm{p,EAT}}T_{\mathrm{EAT}} + \int_0^L h\pi d\,(T - T_{\mathrm{amb}})\,\mathrm{d}l, \tag{10}$$

where C_{p} is the mass-specific heat capacity of the exhaust, h is the heat transfer coefficient between exhaust and surrounding, d is the diameter of the pipe, L is the length of the pipe and l is the axial coordinate of the pipe. Subscripts "cyn", "EAT" and "amb" refers to engine cylinder, EAT system and the ambient respectively. Here radiative heat loss is ignored to maintain the simplicity of the analysis. In addition, the temperature dependence of heat capacity is ignored to further simplify the equation; this would lead to less than 20% error in the relevant temperature range. By using length-averaged h and T yields the following equation:

$$\dot{m}C_{\mathrm{p}}T_{\mathrm{cyn}} = \dot{m}C_{\mathrm{p}}T_{\mathrm{EAT}} + \bar{h}\pi dL\,(\bar{T} - T_{\mathrm{amb}}) \tag{11}$$

Despite many assumptions, we are still left with unknown parameters $\bar{h}$, d, L, $\bar{T}$ and T_{amb}.

For simplicity $\bar{T}$ is chosen to be T_{EAT}; in fact it can be anything between T_{cyn} and T_{EAT}, but there is no real way to tell which is a better estimate. The ambient temperature is assumed to be 25°C. Rearranging eq. (11) for T_{EAT} gives:

$$T_{\mathrm{EAT}} = \frac{1}{\frac{f_{\mathrm{cool}}}{C_{\mathrm{p}}} + \dot{m}} \left(\dot{m} T_{\mathrm{cyn}} + \frac{f_{\mathrm{cool}}}{C_{\mathrm{p}}} T_{\mathrm{amb}} \right), \tag{12}$$

where we lumped unknown parameters into a single parameter $f_{\mathrm{cool}} = h\pi DL$. By choosing f_{cool} to have the value of 214 W/K, all estimated inlet temperature of the EAT system lie within typical range expected [20], as shown in Table 2.

3 Model assessment

In this section, the proposed EAT model is applied to simulate individual EAT devices including a DOC, SCR and DPF. The results of the simulations are compared with experimental and simulation data from literature. The impact of modelling choices with respect to mass transfer phenomena in the proposed model is evaluated.

3.1 Diesel Oxidation Catalyst (DOC)

The main functionality of the DOC is to completely oxidise CO and uHC. It is also capable of promoting NO oxidation subject to thermodynamic constraints. The overall reactions are shown below, where uHC is represented by C_3H_6 [36]:

$$2\,C_3H_6 + 9\,O_2 \longrightarrow 6\,CO_2 + 6\,H_2O \tag{13}$$

$$2\,CO + O_2 \longrightarrow 2\,CO_2 \tag{14}$$

$$2\,NO + O_2 \rightleftharpoons 2\,NO_2 \tag{15}$$

The proposed model is applied to simulate a platinum catalyst experimentally studied by Koop and Deutschmann [36]. They developed a chemical mechanism to describe the redox reactions between platinum and exhaust gas species. They evaluated the performance of the chemical mechanism by simulating the conversion of NO of a platinum catalyst at three different temperatures and two inlet conditions, namely "lean" (12% O_2) and "rich" (0.9% O_2). They showed good agreement between their simulation and their experimental results.

The performance of the proposed model is evaluated by simulating the same set of experiments using the same chemical mechanism. It should be noted there are significant differences between the proposed model and the model used by Koop and Deutschmann [36]. The main difference between the proposed model and the literature model is the

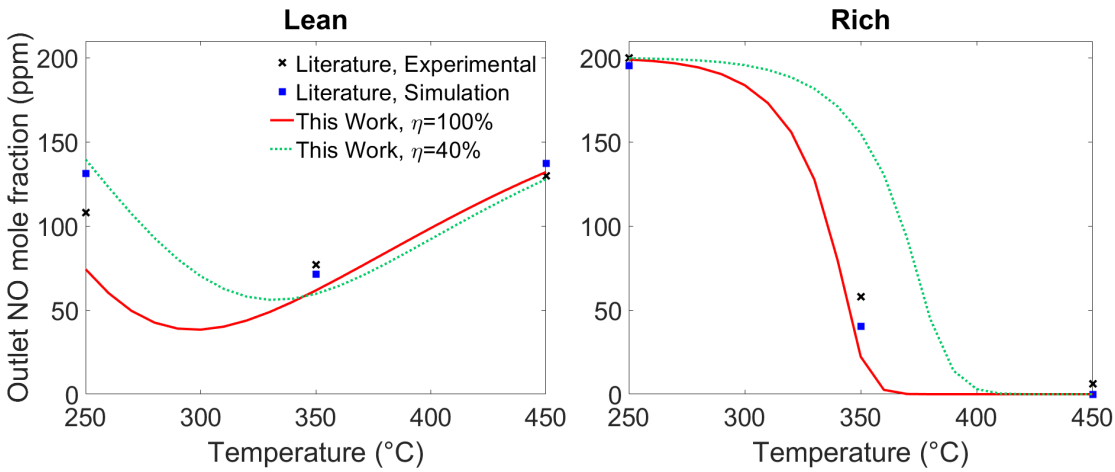

Figure 3: *Comparison of model prediction by the proposed model and literature model [36]. The outlet concentrations of NO under lean and rich conditions agreed qualitatively.*

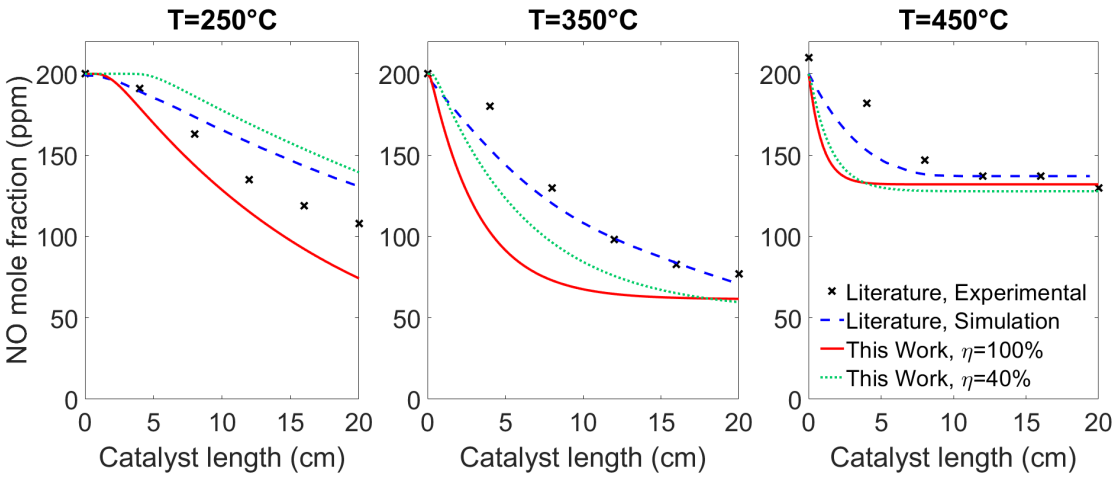

Figure 4: *Comparison of model prediction by the proposed model and literature results [36]. The proposed model is able to describe the axial NO profile along the DOC channel qualitatively under lean conditions.*

treatment for mass transfer phenomena.The literature model considers the catalytic channel using a two-dimensional cylindrical coordinate. As a result, radial mass transfer from the bulk gas flow to the washcoat is solved directly. Furthermore, the diffusion inside the catalytic washcoat was modelled by the effectiveness factor approach by Koop and Deutschmann [36]. In the proposed model, the convective mass transfer is neglected and a global effectiveness factor η is applied to describe the effect of diffusion in the catalytic washcoat.

The experimental measurements and simulations from the literature, as well as predicted outlet NO concentrations made by the proposed after-treatment model are shown in Fig. 3. The axial profiles of NO with "lean" inlet are shown in Fig. 4. Two different values of global effectiveness factor η, 100% and 40%, have been used with the proposed model to

evaluate the impact of washcoat diffusion.

It can be seen from Fig. 3 that using $\eta = 100\%$ works well for the "rich" inlet condition. However it leads to overestimation of the rate of NO oxidation below 350°C for the "lean" inlet, as shown by low NO concentration at the outlet. A better agreement between the proposed model and the literature model can be achieved for the "lean" inlet if η is set to 40%. However, using $\eta = 40\%$ has lead to increased discrepancy between model predictions for the "rich" inlet. It should be noted that the differences between the model predictions can also be attributed to the different treatments for the convective mass transfer between the bulk gas and the catalyst. The impact of convective mass transfer is lumped into the global effectiveness factor in the proposed model. The computational cost of the proposed model would be significantly lower than the literature model due to the one-dimensional axial coordinate description of the DOC, and therefore the trade-off with accuracy in the prediction is deemed acceptable. For the remainder of this study, η is chosen to be 40% for all DOC simulations, since diesel engines are expected to operate under lean-burn condition predominantly.

3.2 Selective Catalytic Reduction (SCR)

The purpose of an NH_3-SCR is to reduce NOx to N_2 by NH_3. There are three major reaction pathways, "standard-SCR" (eq. 16), "fast-SCR" (eq. 17) and "NO_2-SCR" (eq. 18) [49]:

$$4\,NO + 4\,NH_3 + O_2 \longrightarrow 4\,N_2 + 6\,H_2O \tag{16}$$

$$NO + NO_2 + 2\,NH_3 \longrightarrow 2\,N_2 + 3\,H_2O \tag{17}$$

$$6\,NO_2 + 8\,NH_3 \longrightarrow 7\,N_2 + 12\,H_2O \tag{18}$$

NH_3-SCR catalyst formulations are usually based on either Vanadium or Iron/Copper zeolites [13]. As zeolites have better thermal resistance than Vanadium-based catalyst, they are suitable in both SCR-front and DPF-front layouts, whereas Vanadium-based catalyst are only suitable for SCR-front layout [22]. Therefore a Copper zeolite SCR catalyst is chosen for this study.

The chemical mechanism of the Cu-ZSM-5 catalyst developed by Olsson et al. [49] is used in this work. Olsson et al. [49] calibrated the reaction mechanism against various sets of the experimental data. One of the experiments investigated the effect of changing NO-to-NO_2 ratio at the inlet. The inlet concentration underwent step-changes at the time specified in Table 1. The concentrations of NO, NO_2 and N_2O were measured at the outlet.

The proposed model was assessed by simulating the same experiment and comparing the model results with experimental measurements and model predictions made by Olsson et al. [49]. The main difference between the literature model and the proposed model is the treatment for convective mass transfer resistance between the gas flow and the channel wall. An empirical correlation was used by Olsson et al. [49] to describe convective mass

Table 1: *Inlet conditions used in the SCR experiment [49].*

Time (min)	NO (ppm)	NO_2 (ppm)	NH_3 (ppm)	O_2	H_2O	Ar
0	500	0	500	8%	5%	balance
30	400	100	500	8%	5%	balance
45	300	200	500	8%	5%	balance
60	250	250	500	8%	5%	balance
75	200	300	500	8%	5%	balance
90	100	400	500	8%	5%	balance
105	0	500	500	8%	5%	balance

transfer in their model whereas the proposed model assumes kinetic-limited operation, as mentioned above. Olsson et al. [49] concluded that washcoat diffusion was negligible in this case and therefore $\eta = 100\%$ is used. Experimental measurements and predicted concentrations of the literature model and the proposed model are shown in Fig. 5.

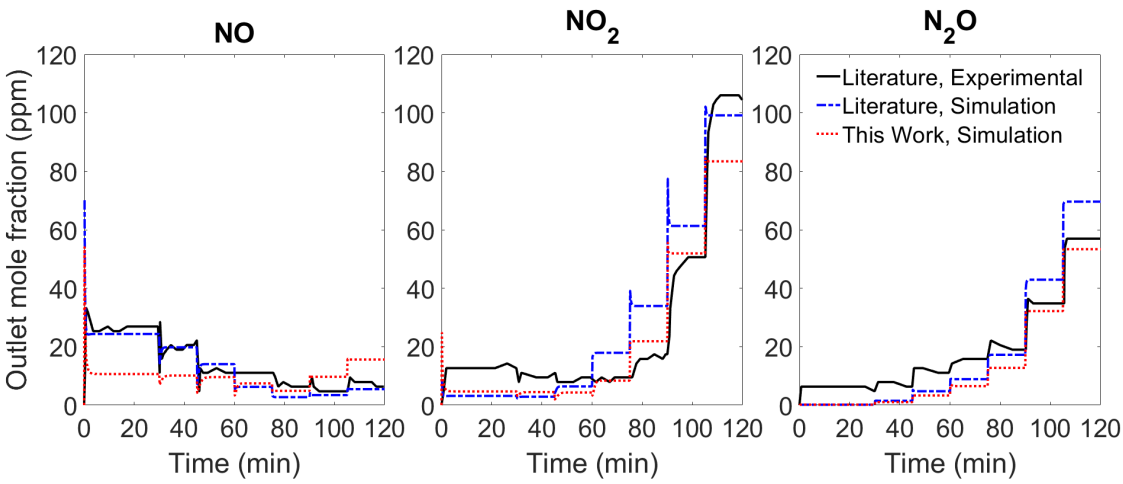

Figure 5: *Comparison of model prediction of NO, NO_2 and N_2O emission by the proposed model and literature results [49].*

Qualitative agreements can be observed between the three sets of data. The differences between predictions by the literature model and the proposed model are attributed to be caused by the absence of convective mass transfer in the proposed model. There is no clear indication in Fig. 5 that the inclusion of the convective mass transfer in the model brings extra benefit. In conclusion, the combination of the chemical mechanism and the proposed model are shown to be able to capture the general trend of the change in NOx conversion, and therefore are sufficient for investigations on the impact of device configurations on overall EAT system design.

3.3 Diesel Particulate Filter (DPF)

It is important to ensure that the proposed model can simulate both the filtration and regeneration process of the DPF with sufficient accuracy. The ability of the proposed model to simulate the filtration behaviour of DPFs is checked against results by Zhang et al. [67] who simulated a DPF that had been studied experimentally by Suresh et al. [59]. The proposed model is applied to predict the change in pressure drop of the DPF as it collects particles, as the pressure drop of the DPF is commonly used in modelling studies to characterise the filtration behaviour [65]. In this work, it is assumed that the inlet particle diameter is 100 nm which is typical for diesel engines [11].

The results of experiment and simulations are shown in Fig. 6, where we can observe excellent agreements between the literature data and predictions by the proposed model.

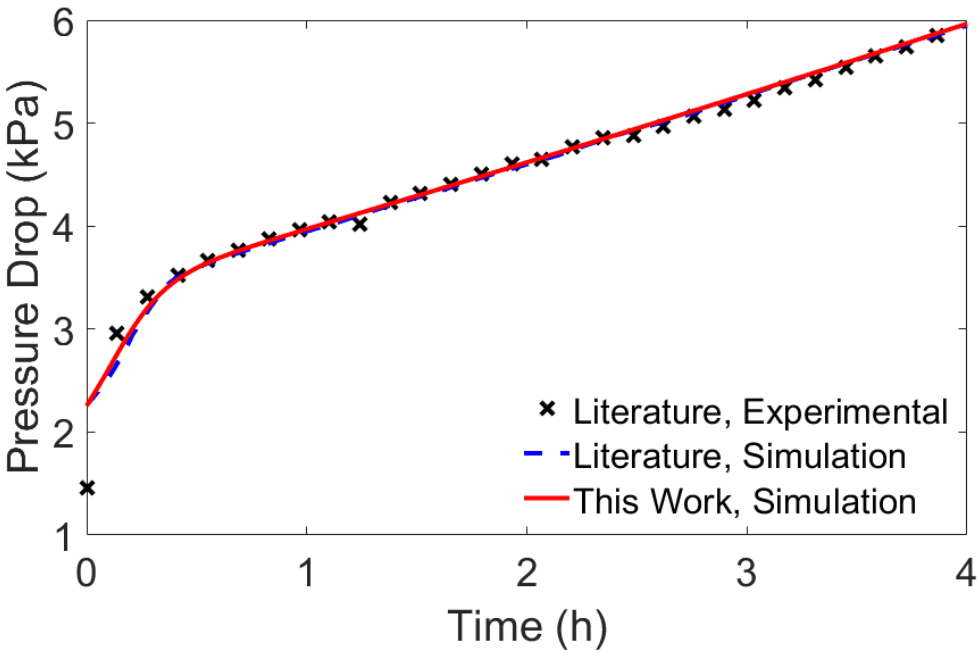

Figure 6: *Comparison of model prediction of DPF backpressure by the proposed model and literature results [59, 67].*

The ability of the proposed model to describe DPFs under active regeneration has been shown in previous work [40]. The rate parameters for active regeneration used in this work are obtained from Bissett [10]. The ability to describe passive regeneration is checked against the work of Kim et al. [29]. They simulated the variation of the mass of trapped particles inside a DPF under three inlet conditions with various NOx-to-PM ratio. The rate parameters for the passive regeneration reactions are calibrated in this work to best reproduce the results of Kim et al. [29]. The predicted particle mass profiles after calibration are shown in Fig. 7. It can be concluded from Fig. 7 that the proposed model is capable of describing the impact of varying NO_2 content on passive regeneration of DPFs.

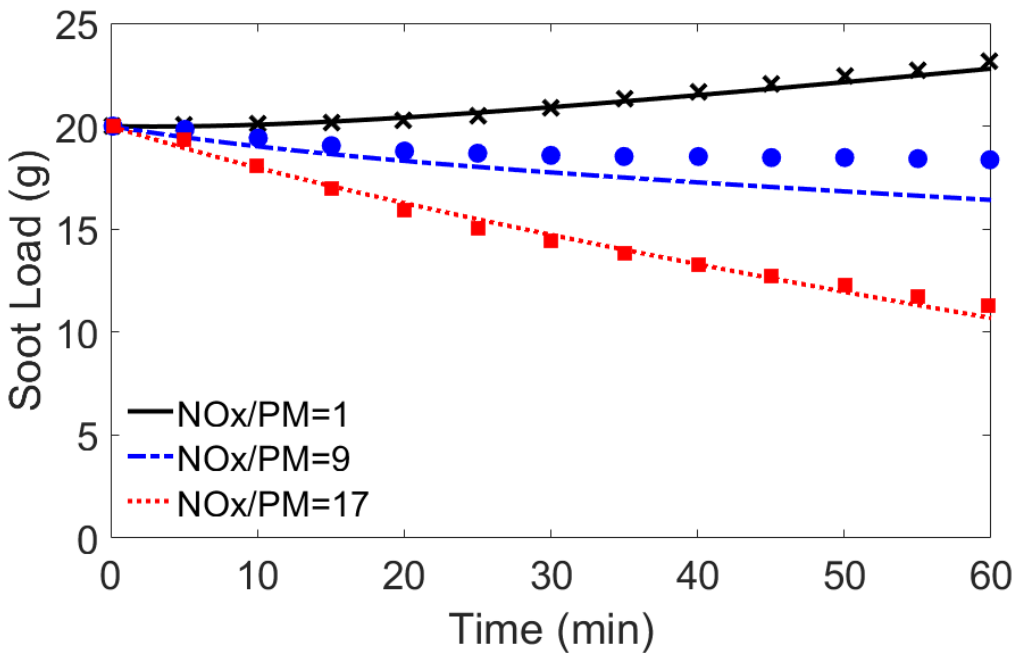

Figure 7: *Comparison of model prediction of soot load during passive regeneration by the proposed model (lines) and the literature model (markers) [29].*

4 Parametric study

In this section, the proposed EAT model is used to investigate interaction between EAT devices in DPF-front and SCR-front EAT systems. The investigation is performed in the context of the design of an EAT system for a heavy-duty diesel engine. First of all, simulations are performed to obtain the engine-out emissions. After that, the proposed EAT model is used to design the EAT system using both a DPF-front and SCR-front layout to meet the appropriate emission standards. The interaction between EAT devices are investigated by evaluation of the system performance and flux analysis.

4.1 Engine simulation

The EAT model is applied to design an EAT system for a heavy-duty diesel engine. This engine model is included in the SRM Engine Suite as "Ex.09 (6 Cylinder 7L HD Diesel LSMap TierIV)". The engine model was calibrated for 8 operating points with varying engine speed and load. The engine-out NOx concentration and the soot emissions are shown on Fig. 8. The Brake Mean Effective Pressure (BMEP) is used as a measure for engine load.

The inlet conditions of the EAT system at the 8 operating points given by the SRM Engine Suite are shown in Table 2. The gas temperature has been corrected using eq. (12).

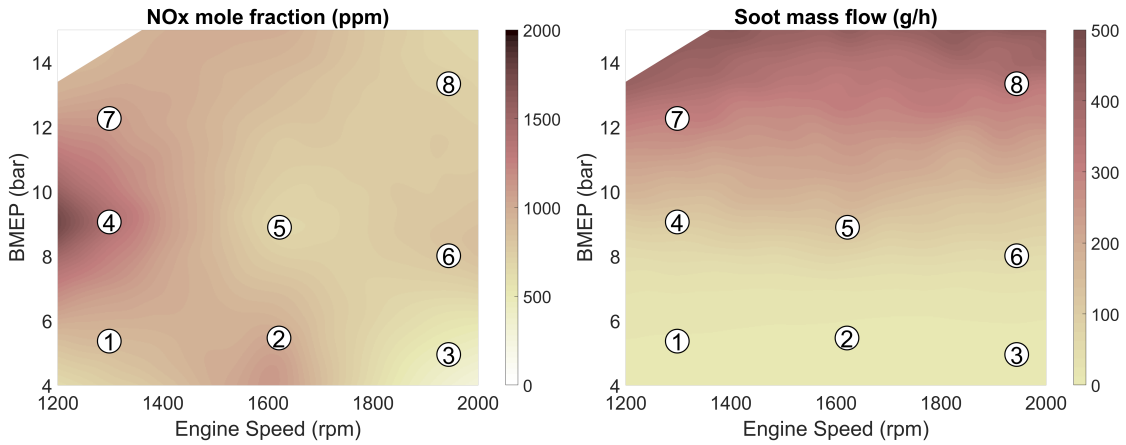

Figure 8: *The predicted NOx and soot emissions of the engine used for the virtual design and testing of the exhaust after-treatment system.*

Table 2: *Inlet conditions of the EAT system studied in this work.*

Operating point	Unit	1	2	3	4	5	6	7	8
Engine speed	rpm	1298	1621	1944	1298	1622	1944	1298	1944
BMEP	bar	5.4	5.5	5.0	9.1	8.9	8.0	12.2	13.3
Gas mass flow	kg/h	363	459	618	425	572	677	569	1027
Gas temperature	°C	204	243	267	297	368	358	375	488
Particle mass flow	kg/h	0.010	0.007	0.004	0.116	0.149	0.059	0.287	0.454
Mass fraction									
CO	ppm	37	39	112	2080	4270	182	7590	6270
CO_2	%	19.8	17.1	21.5	17.6	22.9	23.3	17.9	25.9
H_2O	%	4.5	4.2	4.4	5.6	6.0	5.6	6.1	6.7
O_2	%	11.8	12.4	12.3	8.9	8.1	9.1	7.8	6.6
N_2	%	64	66	62	68	63	62	67	60
NO	ppm	683	805	203	1320	504	677	1030	629
NO_2	ppm	335	359	380	191	193	249	145	171
N_2O	ppm	2.5	2.9	3.7	2.2	2.9	3.1	2.4	3.0
C_3H_6	ppm	16	15	6	65	220	19	1385	1010

4.2 Interaction between after-treatment devices

In this section we examine different EAT systems designs for the 8 operating points listed in Table 2. Both DPF-front and SCR-front layouts are considered. The EAT designs are developed using emission standard IIIB and IV as objectives. The impact of the emissions standard on EAT design and performances can be extracted by comparing the systems behaviours. In order to examine the interaction between after-treatment devices, the lengths of individual devices are varied between designs.

Since large number of design parameters are needed to define an EAT system, thorough analysis is time consuming and may distract us from the objective of this study. Some

simplifications have been applied during the design process so that the investigation can focus on the chemical phenomena. For example, the outer diameter of all EAT devices are fixed to 0.2 m. The catalyst loadings of the DOC and the SCR are chosen to be the same as Section 3.

4.2.1 DPF-front system

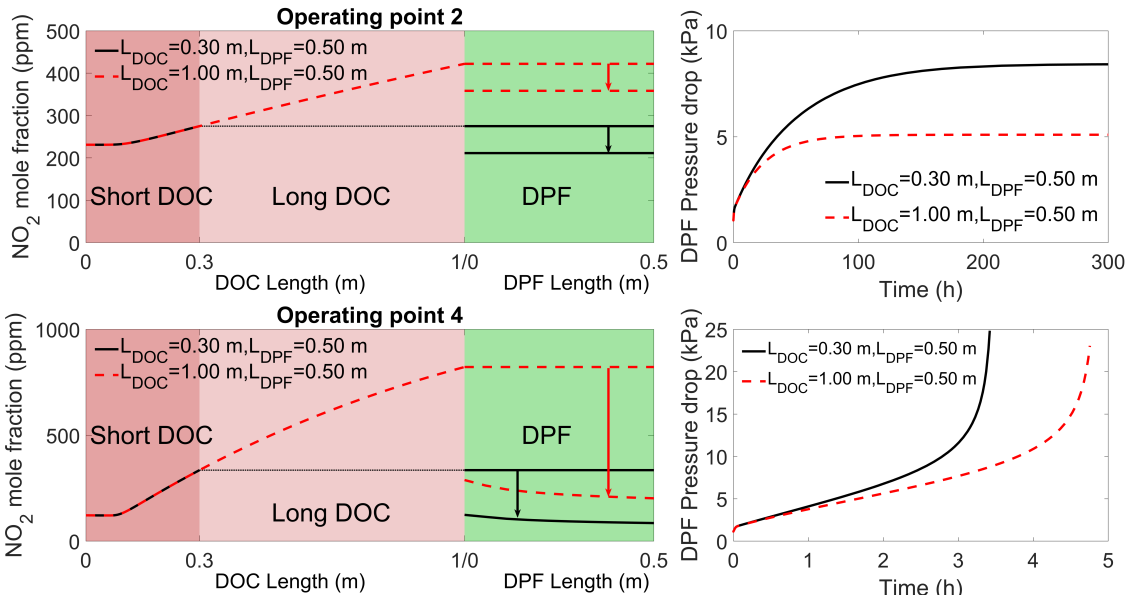

Figure 9: *Impact of the length of upstream DOC on downstream DPF.*

Firstly the interaction between DOC and DPF is examined. This is done by comparing the behaviours of two DOC-DPF systems where the lengths of the DOCs are 0.3 m and 1.0 m respectively. Their behaviours at operating point 2 and 4 are shown in Fig. 9. The concentration profiles of NO_2 are shown here since it is the key reactant for passive regeneration (eq. (9)) of the DPF. NO_2 is generated from NO by the DOC and is consumed subsequently in the DPF. It can be observed from Fig. 9 that increasing the length of the DOC leads to an increase in NO_2 concentration at the inlet of the DPF. At operating point 2, there is sufficient passive regeneration to achieve steady state operation with the short DOC. Steady state operation can also be achieved at operating points 3, 6 and 8. Increasing the length of the DOC results in a lower pressure drop across the DPF, which would have positive implications on the engine cylinder combustion efficiency. This is offset by the increased capital cost of having a longer DOC and an increase in volume of the EAT system, which can be a significant constraint.

At operating point 4, passive regeneration is insufficient to achieve steady state in the system with the short DOC. The inlet channel of the DPF is clogged by particles, resulting in rapid increase in the pressure drop after about 3 hours. Whilst increasing the length of the DOC is also unable to support sufficient regeneration within the DPF, it is capable of delaying clogging by about 1.5 hours. This can reduce the fuel penalty associated with active regeneration. To summarise, increasing the length of the DOC is beneficial

for passive regeneration occurring in the downstream DPF regardless of whether passive regeneration is sufficient to allow continuous operation at a given operating point.

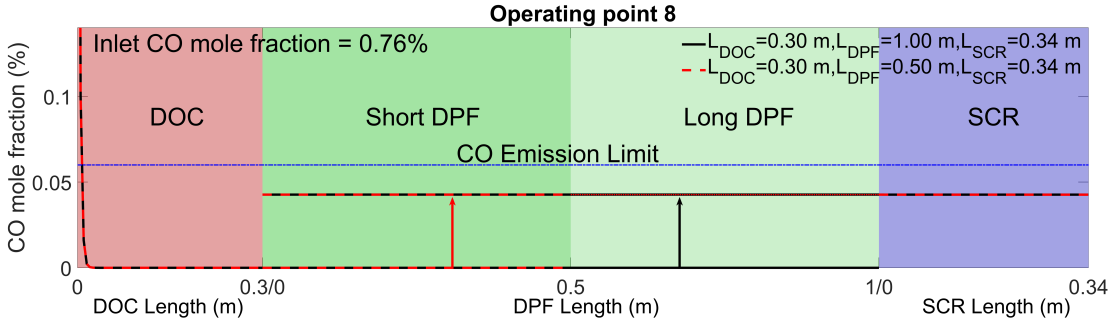

Figure 10: *Secondary CO emission post-DPF due to regeneration.*

Eq. (9) shows that regeneration reactions can lead to production of CO in the exhaust. The implication of this secondary CO emission is demonstrated in Fig. 10, where the CO concentration profiles along two DOC-DPF-SCR systems at operating point 8 are shown. In this case, engine-out CO are completely removed within the DOC. Regeneration reactions inside the DPF leads to an increase of CO in the exhaust. It should be noted that the length of the DPF has no impact on the steady state gas phase composition profile. This secondary CO emission then passes through the downstream SCR catalyst unreacted.

The interaction between CO and the copper zeolite catalyst was not considered during the development of the chemical mechanism in the work of Olsson et al. [49]. It is reported by [66] that copper zeolite catalyst has CO oxidation capability. If this is also possible for the Cu-ZSM-5 catalyst, then the downstream SCR catalyst can prevent CO slip and this makes the DPF-front layout more attractive. Future investigations of SCR catalysts should also consider the possibility of CO oxidation in light of the secondary CO emission.

4.2.2 SCR-front system

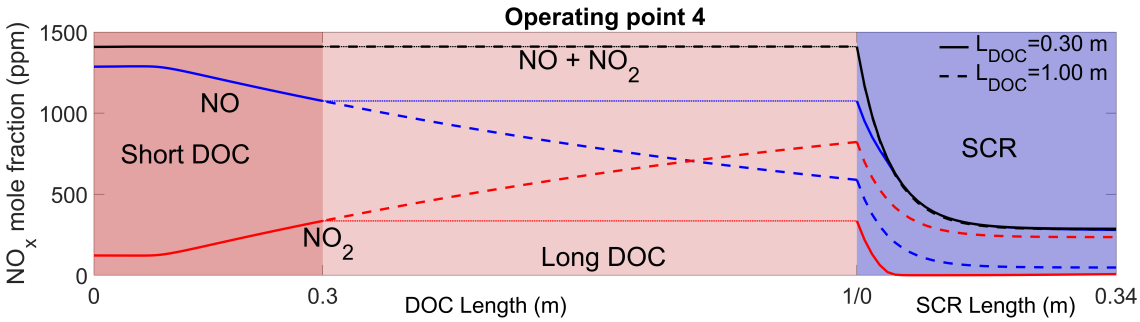

Figure 11: *Impact of the length of upstream DOC on downstream SCR.*

After examining the interaction between the DOC and the DPF, we investigate the interaction between the DOC and the SCR in systems with the SCR-front layout. The DOC can oxidise NO to NO_2, which enables the "fast-SCR" reaction (eq. 17) to be the dominant reaction pathway in the SCR. This claim is examined at operating point 4, where

the concentration profiles of NOx are shown in Fig. 11. Two DOC-SCR systems with two different lengths of DOC are shown here. The NO_2:NOx ratio increased from 0.24 to 0.58 by increasing the length of the DOC from 0.3 m to 1.0 m. It should be noted that the total amount of NOx in the exhaust remains unchanged through the DOC.

Surprisingly, there is little benefit of having a longer DOC. The overall deNOx efficiency is essentially the same for both systems. In order to further investigate the influence of the upstream DOC on the performance of the SCR, flux analysis is applied and the results are discussed in section 4.2.3.

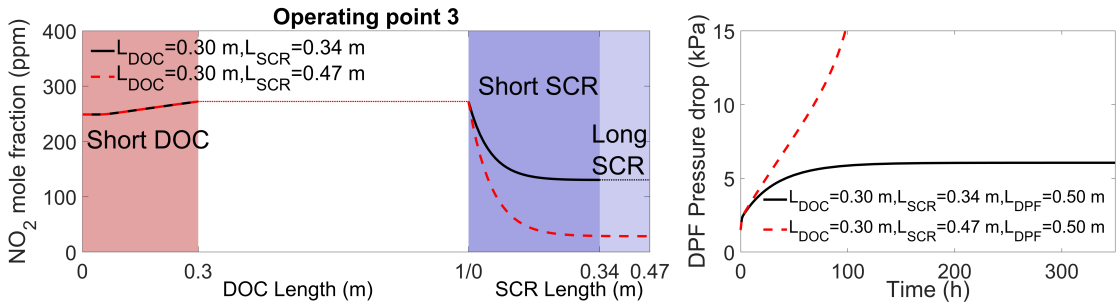

(a) Respective performances of SCR-front systems designed to meet Stage IIIB and Stage IV standard.

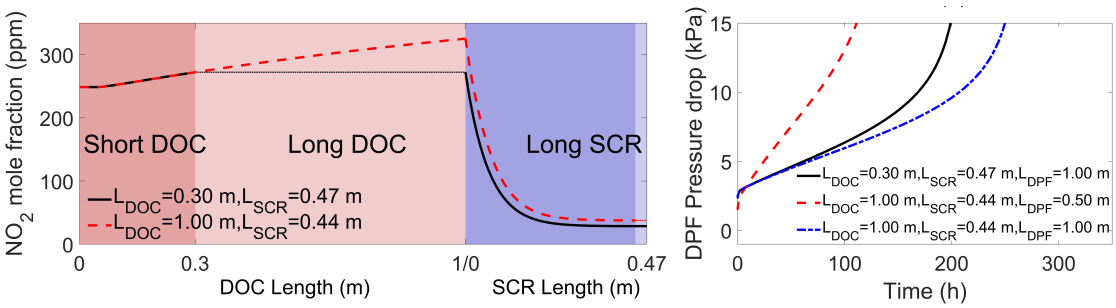

(b) Evaluation of the possibility of sufficient passive regeneration with Stage IV-compliant SCR-front systems.

Figure 12: *Examination of the possibility to have sufficient passive regeneration for steady state operation with SCR-front system.*

Fig. 11 has shown that whilst having a longer DOC has little impact on the overall deNOx efficiency, it increased the amount of NO_2 at the outlet of the SCR, which is the inlet of the DPF in a SCR-front system. This leads to more NO_2 at the exit of the SCR catalyst, which can aid passive regeneration in a downstream DPF. Here we examine the possibility of steady state operation for EAT systems with SCR-front layout. For a Stage IIIB compliant design, it is found that there is sufficient passive regeneration occurring in the DPF to achieve steady state at operating point 3, as shown in Fig. 12(a). In addition, this design is able to achieve steady state at operating point 8.

In order to comply with the Stage IV standard where the NOx limit decreased from 2.0 g/kWh to 0.4 g/kWh [1], the length of the SCR and the amount of NH_3 injection must increase. When the length of the SCR is increased from 0.34 m to 0.47 m, steady state operation is only achievable at operating point 8. At operating point 3, the inlet NO_2 concentration for the DPF has dropped from 130 ppm to 30 ppm, which leads to decreased

regeneration activity in the DPF and ultimately DPF clogging.

Alternative designs are explored to see whether steady state operation in the DPF is possible for a Stage IV compliant SCR-front EAT system. The behaviours of those systems are shown in Fig. 12(b). Firstly the length of the DOC is increased. The length of the SCR has decreased from 0.47 m to 0.44 m correspondingly. However, the impact of the DOC is nullified by the SCR catalyst; the inlet NO_2 concentration for the DPF has only increased from 30 ppm to 40 ppm despite significant increase in DOC size. Fig. 12 shows that steady state operation is not possible, even with a larger DPF, since the size of the DPF does not affect the steady state gas phase composition profile. Similar to previous findings, increasing the length of the DPF can delay clogging but does not mitigate the need for active regeneration.

4.2.3 Flux Analysis

Flux analysis is a technique to investigate reaction mechanisms [48]. It allows better understanding of the behaviour of a system by tracking how elements are "transferred" between chemical species via various reaction pathways. With flux analysis, we can identify the relative importance of the different reaction pathways.

In this case flux analysis is applied to the SCR catalyst with different upstream DOCs at operating point 4. The behaviour of the system is shown in Fig. 11. The fluxes of nitrogen atoms are analysed since SCR is designed to reduce NOx to N_2. Details of the calculations of reaction fluxes can be found in work of Nurkowski et al. [48]. The fluxes of nitrogen atoms inside the SCR at operating point 4 with upstream DOCs of lengths 0.3 m and 1.0 m is shown in Fig. 13.

We can observe that nitrogen atoms "flow" from NOx and NH_3 to N_2 as well as a undesirable by-product N_2O. The net fluxes of nitrogen from adsorbed NH_3 (shown as $NH_3{}^*$ in Fig. 13), NO and NO_2 to N_2 are due to SCR reactions taking place. In addition, the Cu-ZSM-5 catalyst also exhibits NO oxidation activity as reflected by the nitrogen flux from NO to NO_2.

We can clearly see the impact of varying the length of the upstream DOC on the SCR by comparing Fig. 13(a) and 13(b). The fluxes from adsorbed NH_3 to N_2 for both systems are very similar, indicating similar overall deNOx performances. However, the system with the longer DOC would lead to increased amount of NO_2 at the inlet of the SCR, and this leads to corresponding increase in fluxes from NO_2 to N_2 and N_2O. The flux from NO to NO_2 is decreased since the extent of NO oxidation is limited by thermal equilibrium.

Further analysis was performed to study the system behaviour with high inlet NO_2/NOx ratio. It is found that the highest possible NO_2/NOx ratio at the inlet of the SCR is 0.88. This can be achieved if the length of the upstream DOC is increased to 4.15 m, a practically infeasible sizing. The nitrogen fluxes are shown as stacked bars on Fig. 14. The contributions of standard SCR, fast SCR and NO_2 SCR as well as the N_2O producing side-reaction vary with the inlet NO_2/NOx ratio.

In addition to the nitrogen fluxes shown on the left vertical axis, the deNOx efficiencies under different inlet NOx ratio at four NH_3 dosage levels are shown as curves on the

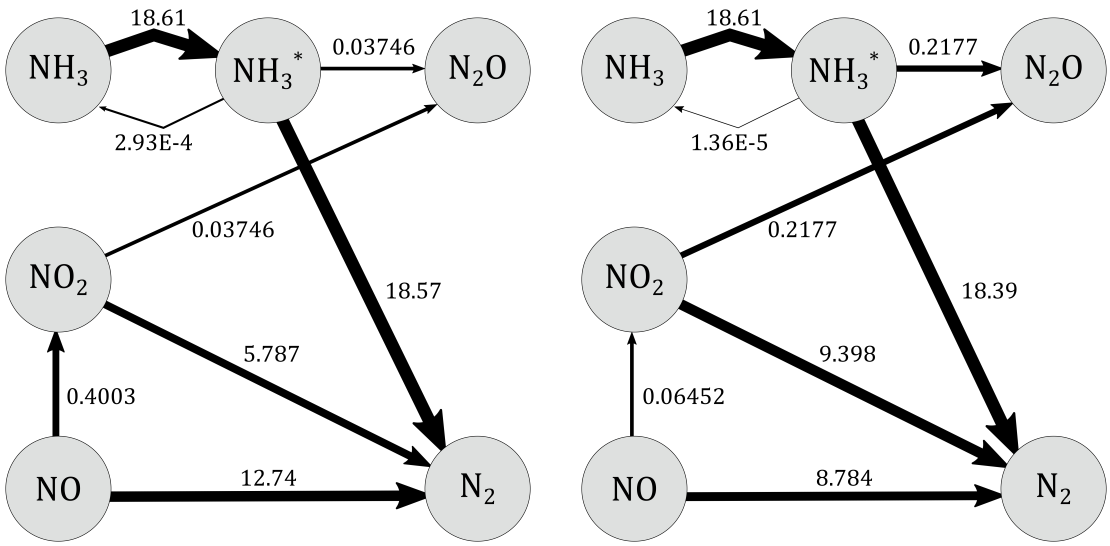

(a) Flux with DOC length 0.3 m.

(b) Flux with DOC length 1.0 m.

Figure 13: *Flux of Nitrogen in the SCR with upstream DOCs of lengths 0.3 m and 1.0 m at operating point 4. The fluxes of nitrogen atoms (mol/m^{3}s) are integrated along the entire length of the SCR.*

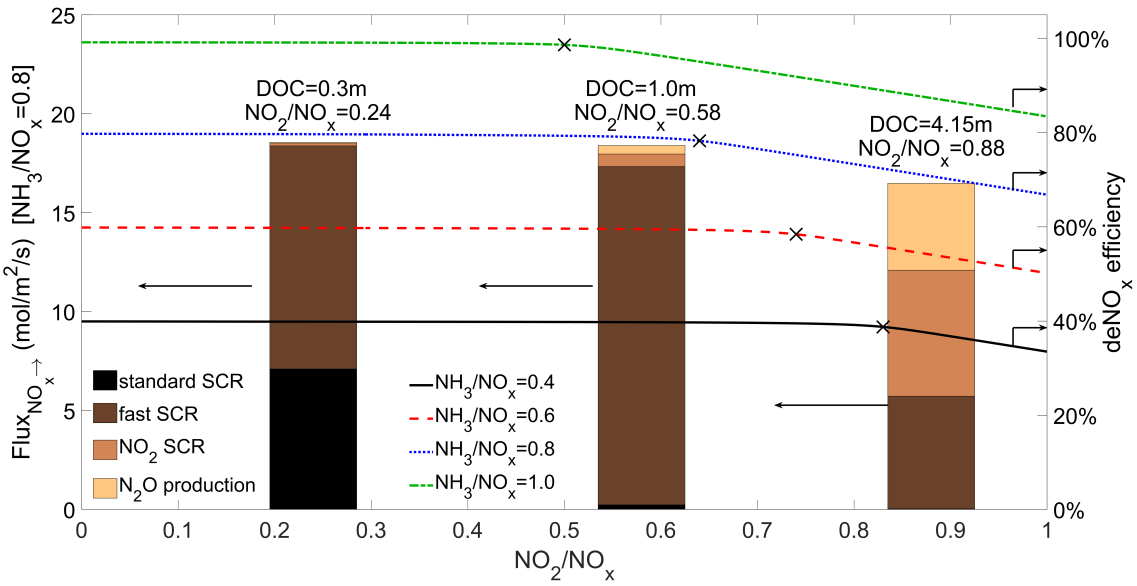

Figure 14: *The variation in deNOx efficiency of the SCR with different inlet NO_2/NOx. The fluxes of nitrogen atoms from NOx to other species are shown as stacked bars for three DOC-SCR systems. The nitrogen flux correlates to the efficiency of the SCR. The critical NO_2/NOx ratio for each NH_3 dosing are shown as crosses.*

right vertical axis. The deNOx efficiencies are at their respective minimum when the inlet contains 100% NO_2. By reducing the amount of NO_2 at the inlet, the SCR becomes more

efficient. The critical NO_2/NOx ratio for maximum deNOx efficiency is marked on the four efficiency curves.

It is observed that the total nitrogen flux from NOx correlates with the deNOx efficiency. The decrease in efficiency at high NO_2 content can be explained by the individual flux contributions. The contributions of the fast SCR and the standard SCR to NOx removal are lowest when the $NO_2/NOx = 0.88$ at the SCR inlet. Furthermore, the flux of N_2O production is the highest, which is undesirable since N_2O is a strong greenhouse gas [13].

The results of flux analysis can shed light on decisions needed when designing EAT systems. In this case, increasing the length of the DOC to 1.0 m has little benefit on the downstream SCR since the increased activity of fast SCR reaction is counter-balanced by the decrease in standard SCR activity. Whilst these conclusions are limited to this particular catalyst, flux analysis have been shown to be useful for other EAT design problems.

4.2.4 Comparison between DPF-front and SCR-front layout

It is apparent that the DPF-front system is superior with respect to the SCR-front system in terms of regeneration strategy. The DPF-front system is able to achieve steady state with sufficient passive regeneration activities for 4 out of 8 operating points investigated. On the other hand the Stage IIIB compliant SCR-front system can only reach steady state at 2 operating points. Passive regeneration activities can reduce the fuel penalties associated with active regeneration. When emission standards become more stringent, passive regeneration in the SCR-front system is further limited as shown in Fig. 12. This implies an increase in the need for active regeneration. Furthermore, the CO generated from DPF regeneration may be treated by the downstream SCR catalyst in a DPF-front system, since the copper zeolite catalyst may be able to oxidise CO. This remains to be investigated.

Whilst more NO_2 is available to the SCR in SCR-front systems, the overall deNOx efficiency is not improved. Flux analysis in Section 4.2.3 has shown that the benefit of increased fast SCR activity due to higher NO_2 content is cancelled by a decrease in standard SCR activity.

In conclusion, the DPF-front layout has been shown to have better steady state performance compared to the SCR-front layout in this case study. The benefit of higher passive regeneration activities is clearly shown, whereas an increase of the fast SCR activity has no significant impact on the overall deNOx performance of the EAT system under steady state operation.

5 Conclusions

A single channel EAT model with rigorous treatment for the catalytic chemistry has been proposed in this study. The performances of the proposed model for simulating a DOC, SCR and DPF are compared with experimental and simulation data from the literature. The proposed model has been shown to be able to describe the behaviours of relevant after-treatment devices with sufficient accuracy given the simplified treatment for mass transfer phenomena. The proposed model is then applied to design after-treatment systems for

a heavy duty diesel engine simulated using virtual engine software. The steady state behaviours of designs with different configurations, emission standards requirements and lengths of individual devices are investigated.

The DOC is found to promote passive regeneration in a downstream DPF which may be able to be exploited to reduce the fuel penalty associated with active regeneration frequency and backpressure. However, it is not always possible to achieve steady state operation of the passive regeneration by increasing the size of the DOC. Furthermore, increased regeneration activity could lead to significant secondary CO emissions post-DPF which cannot be treated by the DOC. This study has not found the reportedly positive impact of an upstream DOC on the SCR catalyst [14]. Further flux analysis suggests that the particular SCR catalyst studied is insensitive to the NO_2 portion at its inlet, for the range of possible inlet species concentrations provided by the DOCs considered in this design study.

It was found that as more stringent emission standards are adopted, the possibility of passive regeneration is reduced for SCR-front EAT systems. The NOx emission limits constrains the sizing of the SCR catalyst, which is the only device with net NOx conversion along after-treatment devices included in this study. In addition, it is possible that the SCR catalyst exhibits CO oxidation activity and therefore the SCR catalyst can help to mitigate secondary CO emissions due to DPF regeneration in a DPF-front system. To summarise, the DPF-front design is superior to the SCR-front design for this case study, and it is expected to become more popular in the future.

This study has focused on the steady state performance of the EAT systems. Future studies should be extended to consider transient and thermal behaviour of EAT systems under more complicated operating conditions including cold-start behaviour and active regeneration. The numerical model should be further developed to be able to simulate more advanced, integrated EAT devices such as catalysed particulate filters and dual-layer catalysts.

Acknowledgements

The authors would like to thank Cambridge Centre for Advanced Research and Education in Singapore (CARES), Engineering and Physical Sciences Research Council (EPSRC) and Royal Dutch Shell for their support. This project has received funding from the European Union's Horizon 2020 Research and Innovation Programme under grant agreement no. 724145.

Nomenclature

Roman symbols	Meaning	Unit
A	Pre-exponential constant	(mol,cm,s)
B	Temperature exponent	-
C_p	Specific heat capacity	kJ/kgK
c	Molar concentration of gas species	mol/m^3
D	Side length of square channel cross-section	m
d	Diameter	m
d_p	Diameter of particle	m
E	Activation energy	kJ/mol
F	Friction factor	-
f_cool	Cooling factor	W/K
h	Heat transfer coefficient	W/m^{2}K
J	Total number of connections	-
k	Reaction rate constant	(mol,cm,s)
L	Length between centres of adjacent volume elements	m
l	Axial coordinate	m
M	Molar mass	kg/mol
$\dot{m}$	Gas mass flow rate	kg/s
N	Particle number density	1/m^3
$\dot{N}$	Flow rate of particle number density	1/m^{3}s
n	Number of mole	mol
P	Pressure	Pa
Q	Filtration efficiency	-
R	Universal gas constant	kJ/molK
r	Rate of reaction	mol/m^{3}s
S	Reactive surface area	m^2
T	Temperature	K
t	Time	s
u	Channel gas flow velocity	m/s
V	Volume	m^3
W	Total number of reactions	-
v	Through-wall gas flow velocity	m/s
X	Reaction order	-
Y	Mass fraction of gas species	-

Greek symbols	Meaning	Unit
α	Stoichiometric constant for regeneration	-
Γ	Total number of gas phase species	-
ζ	Surface concentration	mol/m^2
η	Effectiveness factor	-
θ	Site fraction	-
κ	Permeability	m^2
μ	Gas viscosity	Pa.s
ν	Stoichiometric coefficient	-
ρ	Dynamic density	kg/m^3
σ	Coverage dependent parameter	-
Ψ	Total number of surface species	-

Subscript	Meaning
i	Volume element index
w	Reaction index
γ	Gas species index
β	Surface species index
z	Particle size class index
amb	Ambient
in	Inlet
out	Outlet
cyn	Engine cylinder
AR	Active regeneration
PR	Passive regeneration

References

[1] Directive 2004/26/EC of the European Parliament and of the Council of 21 April 2004 amending Directive 97/68/EC on the approximation of the laws of the Member States relating to measures against the emission of gaseous and particulate pollutants from internal combustion engines to be installed in non-road mobile machinery, 2004.

[2] https://www.acea.be/uploads/statistic_documents/Economic_and_Market_Report_Q2_2018.pdf, 2018.

[3] https://www.acea.be/uploads/statistic_documents/ACEA_Report_Vehicles_in_use-Europe_2018.pdf, 2018.

[4] M. Ahmadinejad, M. R. Desai, T. C. Watling, and A. P. York. Simulation of automotive emission control systems. *Automotive Emission Control*, 33(07):47–101, 2007. doi:10.1016/S0065-2377(07)33002-0.

[5] M. Balthasar, F. Mauss, A. Knobel, and M. Kraft. Detailed modeling of soot formation in a partially stirred plug flow reactor. *Combustion and Flame*, 128(4):395 – 409, 2002. doi:10.1016/S0010-2180(01)00344-3.

[6] S. Bensaid, C. J. Caroca, N. Russo, and D. Fino. Detailed investigation of non-catalytic DPF regeneration. *Canadian Journal of Chemical Engineering*, 89(2):401–407, 2011. doi:10.1002/cjce.20408.

[7] A. Bhave and M. Kraft. Partially stirred reactor model: Analytical solutions and numerical convergence study of a pdf/monte carlo method. *SIAM Journal on Scientific Computing*, 25(5):1798–1823, 2004. doi:10.1137/S1064827502411328.

[8] A. Bhave, M. Balthasar, M. Kraft, and F. Mauss. Analysis of a natural gas fuelled homogeneous charge compression ignition engine with exhaust gas recirculation using a stochastic reactor model. *International Journal of Engine Research*, 5(1):93–104, 2004. doi:10.1243/146808704772914273.

[9] A. Bhave, M. Kraft, L. Montorsi, and F. Mauss. Sources of CO emissions in an HCCI engine: A numerical analysis. *Combustion and Flame*, 144(3):634–637, 2006. doi:10.1016/j.combustflame.2005.10.015.

[10] E. J. Bissett. Mathematical model of the thermal regeneration of a wall-flow monolith diesel particulate filter. *Chemical Engineering Science*, 39(7-8):1233–1244, 1984. doi:10.1016/0009-2509(84)85084-8.

[11] J. C. Caroca, F. Millo, D. Vezza, T. Vlachos, A. De Filippo, S. Bensaid, N. Russo, and D. Fino. Detailed Investigation on Soot Particle Size Distribution during DPF Regeneration, using Standard and Bio-Diesel Fuels. *Industrial & Engineering Chemistry Research*, 50(5):2650–2658, 2011. doi:10.1021/ie1006799.

[12] J. Chen, H. Yang, N. Wang, Z. Ring, and T. Dabros. Mathematical modeling of monolith catalysts and reactors for gas phase reactions. *Applied Catalysis A: General*, 345(1):1–11, 2008. doi:10.1016/j.apcata.2008.04.010.

[13] C. P. Cho, Y. D. Pyo, J. Y. Jang, G. C. Kim, and Y. J. Shin. NOx reduction and N_2O emissions in a diesel engine exhaust using fe-zeolite and vanadium based scr catalysts. *Applied Thermal Engineering*, 110:18–24, 2017. doi:10.1016/j.applthermaleng.2016.08.118.

[14] C. Ciardelli, I. Nova, E. Tronconi, D. Chatterjee, B. Bandl-Konrad, M. Weibel, and B. Krutzsch. Reactivity of NO/NO_2-NH_3 SCR system for diesel exhaust aftertreatment: Identification of the reaction network as a function of temperature and NO_2 feed content. *Applied Catalysis B: Environmental*, 70(1-4):80–90, 2007. doi:10.1016/j.apcatb.2005.10.041.

[15] CMCL Innovations. SRM Engine Suite, 2019.

[16] V. D. Dasireddy and B. Likozar. Selective catalytic reduction of NOx by CO over bimetallic transition metals supported by multi-walled carbon nanotubes (MWCNT). *Chemical Engineering Journal*, 326:886–900, 2017. doi:10.1016/j.cej.2017.06.019.

[17] C. Depcik and D. Assanis. One-dimensional automotive catalyst modeling. *Progress in Energy and Combustion Science*, 31(4):308–369, 2005. doi:10.1016/j.pecs.2005.08.001.

[18] W. S. Epling, L. E. Campbell, A. Yezerets, N. W. Currier, and J. E. Parks. Overview of the fundamental reactions and degradation mechanisms of NOx storage/reduction catalysts. *Catal. Rev. Sci. Eng.*, 46(2):163–245, 2004. doi:10.1081/cr-200031932.

[19] J. Etheridge, S. Mosbach, M. Kraft, H. Wu, and N. Collings. Modelling soot formation in a DISI engine. *Proceedings of the Combustion Institute*, 33(2):3159–3167, 2011. doi:10.1016/j.proci.2010.07.039.

[20] D. Fino, S. Bensaid, M. Piumetti, and N. Russo. A review on the catalytic combustion of soot in Diesel particulate filters for automotive applications: From powder catalysts to structured reactors. *Applied Catalysis A: General*, 509:75–96, 2016. doi:10.1016/j.apcata.2015.10.016.

[21] P. Forzatti, L. Lietti, I. Nova, and E. Tronconi. Diesel NOx aftertreatment catalytic technologies: Analogies in LNT and SCR catalytic chemistry. *Catalysis Today*, 151 (3-4):202–211, 2010. doi:10.1016/j.cattod.2010.02.025.

[22] B. Guan, R. Zhan, H. Lin, and Z. Huang. Review of state of the art technologies of selective catalytic reduction of NOx from diesel engine exhaust. *Applied Thermal Engineering*, 66(1-2):395–414, 2014. doi:10.1016/j.applthermaleng.2014.02.021.

[23] B. Guan, R. Zhan, H. Lin, and Z. Huang. Review of the state-of-the-art of exhaust particulate filter technology in internal combustion engines. *Journal of Environmental Management*, 154:225–258, 2015. doi:10.1016/j.jenvman.2015.02.027.

[24] A. Gurupatham and Y. He. Architecture Design and Analysis of Diesel Engine Exhaust Aftertreatment System and Comparative Study with Close-coupled DOC-DPF System. *SAE Int. J. Fuels Lubr.*, 1(1):1387–1396, 2008. doi:10.4271/2008-01-1756.

[25] S. K. Hoekman and C. Robbins. Review of the effects of biodiesel on NOx emissions. *Fuel Processing Technology*, 96:237–249, 2012. doi:10.1016/j.fuproc.2011.12.036.

[26] G. T. Kalghatgi. Developments in internal combustion engines and implications for combustion science and future transport fuels. *Proceedings of the Combustion Institute*, 35(1):101–115, 2015. doi:10.1016/j.proci.2014.10.002.

[27] S. H. Kamble, T. V. Mathew, and G. Sharma. Development of real-world driving cycle: Case study of Pune, India. *Transportation Research Part D: Transport and Environment*, 14(2):132–140, 2009. doi:10.1016/j.trd.2008.11.008.

[28] I. P. Kandylas and G. C. Koltsakis. NO_2-assisted regeneration of diesel particulate filters: A modeling study. *Industrial & Engineering Chemistry Research*, 41(9): 2115–2123, 2002. doi:10.1021/ie010842m.

[29] J. H. Kim, M. Y. Kim, and H. G. Kim. NO_2-assisted soot regeneration behavior in a diesel particulate filter with heavy-duty diesel exhaust gases. *Numerical Heat Transfer, Part A: Applications*, 58(9):725–739, 2010. doi:10.1080/10407782.2010.523293.

[30] K. H. Kim, E. Kabir, and S. Kabir. A review on the human health impact of airborne particulate matter. *Environment International*, 74:136–143, 2015. doi:10.1016/j.envint.2014.10.005.

[31] M. K. Kim, P. S. Kim, H. J. Kwon, I. S. Nam, B. K. Cho, and S. H. Oh. Simulation of OHC/SCR process over Ag/Al_2O_3 catalyst for removing NOx from diesel engine. *Chemical Engineering Journal*, 209:280–292, 2012. doi:10.1016/j.cej.2012.08.002.

[32] T. Kirchner and G. Eigenberger. Optimization of the cold-start behaviour of automotive catalysts using an electrically heated pre-catalyst. *Chemical Engineering Science*, 51(10):2409–2418, 1996. doi:10.1016/0009-2509(96)00097-8.

[33] E. Kladopoulou, S. Yang, J. Johnson, G. Parker, and A. G. Konstandopoulos. A study describing the performance of diesel particulate filters during loading and regeneration: A lumped parameter model for control applications. *SAE transactions*, 112(724):647–668, 2003. doi:10.4271/2003-01-0842.

[34] J. Ko, W. Si, D. Jin, C.-L. Myung, and S. Park. Effect of active regeneration on time-resolved characteristics of gaseous emissions and size-resolved particle emissions from light-duty diesel engine. *Journal of Aerosol Science*, 91:62–77, 2016. doi:10.1016/j.jaerosci.2015.09.007.

[35] A. G. Konstandopoulos and M. Kostoglou. Reciprocating flow regeneration of soot filters. *Combustion and Flame*, 121(3):488–500, 2000. doi:10.1016/S0010-2180(99)00156-X.

[36] J. Koop and O. Deutschmann. Detailed surface reaction mechanism for Pt-catalyzed abatement of automotive exhaust gases. *Applied Catalysis B: Environmental*, 91 (1-2):47–58, 2009. doi:10.1016/j.apcatb.2009.05.006.

[37] A. S. Kota, D. Luss, and V. Balakotaiah. Micro-kinetics of NOx storage and reduction with H_2/CO/C_3H_6 on Pt/BaO/Al_2O_3 monolith catalysts. *Chemical Engineering Journal*, 262:541–551, 2015. doi:10.1016/j.cej.2014.09.060.

[38] M. Kraft. Stochastic modeling of turbulent reacting flow in chemical engineering, Oct 1998.

[39] M. Kraft, P. Maigaard, F. Mauss, M. Christensen, and B. Johansson. Investigation of combustion emissions in a homogeneous charge compression injection engine: Measurements and a new computational model. *Proceedings of the Combustion Institute*, 28(1):1195 – 1201, 2000. doi:10.1016/S0082-0784(00)80330-6.

[40] C. T. Lao, J. Akroyd, N. Eaves, A. Smith, N. Morgan, A. Bhave, and M. Kraft. Modelling particle mass and particle number emissions during the active regeneration of diesel particulate filters. *Proceedings of the Combustion Institute*, 37(4):4831–4838, 2019. doi:10.1016/j.proci.2018.07.079.

[41] J. Lelieveld, J. S. Evans, M. Fnais, D. Giannadaki, and A. Pozzer. The contribution of outdoor air pollution sources to premature mortality on a global scale. *Nature*, 525(7569):367–371, 2015. doi:10.1038/nature15371.

[42] P. Maigaard, F. Mauss, and M. Kraft. Homogeneous charge compression ignition engine: A simulation study on the effects of inhomogeneities. *Journal of Engineering for Gas Turbines and Power*, 125(2):466 – 471, 2003. doi:10.1115/1.1563240.

[43] N. Morgan, A. Smallbone, A. Bhave, M. Kraft, R. Cracknell, and G. Kalghatgi. Mapping surrogate gasoline compositions into ron/mon space. *Combustion and Flame*, 157(6):1122 – 1131, 2010. doi:10.1016/j.combustflame.2010.02.003.

[44] S. Mosbach, H. Su, M. Kraft, A. Bhave, F. Mauss, Z. Wang, and J.-X. Wang. Dual injection homogeneous charge compression ignition engine simulation using a stochastic reactor model. *International Journal of Engine Research*, 8(1):41–50, 2007. doi:10.1243/14680874JER01806.

[45] S. Mosbach, M. S. Celnik, A. Raj, M. Kraft, H. R. Zhang, S. Kubo, and K.-O. Kim. Towards a detailed soot model for internal combustion engines. *Combustion and Flame*, 156(6):1156 – 1165, 2009. doi:10.1016/j.combustflame.2009.01.003.

[46] L. Mukadi and R. Hayes. Modelling the three-way catalytic converter with mechanistic kinetics using the Newton-Krylov method on a parallel computer. *Computers & Chemical Engineering*, 26(3):439–455, 2002. doi:10.1016/S0098-1354(01)00763-3.

[47] J. Neeft. Kinetics of the oxidation of diesel soot. *Fuel*, 76(12):1129–1136, 1997. doi:10.1016/S0016-2361(97)00119-1.

[48] D. Nurkowski, P. Buerger, J. Akroyd, and M. Kraft. A detailed kinetic study of the thermal decomposition of tetraethoxysilane. *Proceedings of the Combustion Institute*, 35(2):2291–2298, 2015. doi:10.1016/j.proci.2014.06.093.

[49] L. Olsson, H. Sjövall, and R. J. Blint. A kinetic model for ammonia selective catalytic reduction over Cu-ZSM-5. *Applied Catalysis B: Environmental*, 81(3-4):203–217, 2008. doi:10.1016/j.apcatb.2007.12.011.

[50] Y. K. Park, P. Aghalayam, and D. G. Vlachos. A Generalized Approach for Predicting Coverage-Dependent Reaction Parameters of Complex Surface Reactions: Application to H_2 Oxidation over Platinum. *Journal of Physical Chemistry A*, 103: 8101–8107, 1999. doi:10.1021/jp9916485.

[51] F. Payri, P. Olmeda, F. J. Arnau, A. Dombrovsky, and L. Smith. External heat losses in small turbochargers: Model and experiments. *Energy*, 71:534–546, 2014. doi:10.1016/j.energy.2014.04.096.

[52] V. Ramanathan, G. Carmichael, V. Ramanathan and G. Carmichael, V. Ramanathan, and G. Carmichael. Global and regional climate changes due to black carbon. *Nature Geoscience*, 1(4):221 – 227, 2008. doi:10.1038/ngeo156.

[53] R. Ramdas, E. Nowicka, R. Jenkins, D. Sellick, C. Davies, and S. Golunski. Using real particulate matter to evaluate combustion catalysts for direct regeneration of diesel soot filters. *Applied Catalysis B: Environmental*, 176:436–443, 2015. doi:10.1016/j.apcatb.2015.04.031.

[54] İ. A. Reşitoğlu, K. Altinişik, and A. Keskin. The pollutant emissions from diesel-engine vehicles and exhaust aftertreatment systems. *Clean Technologies and Environmental Policy*, 17(1):15–27, 2014. doi:10.1007/s10098-014-0793-9.

[55] D. Rothe, M. Knauer, G. Emmerling, D. Deyerling, and R. Niessner. Emissions during active regeneration of a diesel particulate filter on a heavy duty diesel engine: Stationary tests. *Journal of Aerosol Science*, 90:14–25, 2015. doi:10.1016/j.jaerosci.2015.07.007.

[56] S. Roy and A. Baiker. NOx Storage - Reduction Catalysis : From Mechanism and Materials Properties to Storage - Reduction Performance. *Chemical Reviews*, 109 (9):4054–4091, 2009. doi:10.1021/cr800496f.

[57] M. Schejbal, M. Marek, M. Kubíček, and P. Kočí. Modelling of diesel filters for particulates removal. *Chemical Engineering Journal*, 154(1-3):219–230, 2009. doi:10.1016/j.cej.2009.04.056.

[58] M. Schejbal, J. Štěpánek, M. Marek, P. Kočí, and M. Kubíček. Modelling of soot oxidation by NO_2 in various types of diesel particulate filters. *Fuel*, 89(9):2365–2375, 2010. doi:10.1016/j.fuel.2010.04.018.

[59] A. Suresh, A. Khan, and J. H. Johnson. An Experimental and Modeling Study of Cordierite Traps - Pressure Drop and Permeability of Clean and Particulate Loaded Traps. *SAE Technical Paper Series*, 2000, 2000. doi:10.4271/2000-01-0476.

[60] G. Triantafyllopoulos, D. Katsaounis, D. Karamitros, L. Ntziachristos, and Z. Samaras. Experimental assessment of the potential to decrease diesel NOx emissions beyond minimum requirements for Euro 6 Real Drive Emissions (RDE) compliance. *Science of the Total Environment*, 618:1400–1407, 2017. doi:10.1016/j.scitotenv.2017.09.274.

[61] M. Tutuianu, P. Bonnel, B. Ciuffo, T. Haniu, N. Ichikawa, A. Marotta, J. Pavlovic, and H. Steven. Development of the World-wide harmonized Light duty Test Cycle (WLTC) and a possible pathway for its introduction in the European legislation. *Transportation Research Part D: Transport and Environment*, 40:61–75, 2015. doi:10.1016/j.trd.2015.07.011.

[62] S. E. Voltz, C. R. Morgan, D. Liederman, and S. M. Jacob. Kinetic Study of Carbon Monoxide and Propylene Oxidation on Platinum Catalysts. *Industrial & Engineering Chemistry Product Research and Development*, 12(4):294–301, 1973. doi:10.1021/i360048a006.

[63] B. Wang, S. Mosbach, S. Schmutzhard, S. Shuai, Y. Huang, and M. Kraft. Modelling soot formation from wall films in a gasoline direct injection engine using a detailed population balance model. *Applied Energy*, 163:154–166, 2016. doi:10.1016/j.apenergy.2015.11.011.

[64] K. Yamamoto and Y. Kanamori. Measurements of size distribution and oxidation rate of pm with NO_2. *SAE Technical Paper*, 2015. doi:10.4271/2015-01-1995.

[65] S. Yang, C. Deng, Y. Gao, and Y. He. Diesel particulate filter design simulation: A review. *Advances in Mechanical Engineering*, 8(3):1–14, 2016. doi:10.1177/1687814016637328.

[66] D. Zhang, H. Zhang, and Y. Yan. Copper-ceria catalysts supported on NaX zeolite for CO oxidation. *Microporous and Mesoporous Materials*, 243:193–200, 2017. doi:10.1016/j.micromeso.2017.02.016.

[67] Z. Zhang, S. L. Yang, and J. H. Johnson. Modeling and Numerical Simulation of Diesel Particulate Trap Performance During Loading and Regeneration. *SAE Technical Paper*, (724):2002–01–1019, 2002. doi:10.4271/2002-01-1019.

Citation index